Cavity approach to the spectral density of sparse symmetric random matrices

Tim Rogers, Isaac Pérez Castillo, and Reimer Kühn
Department of Mathematics, King's College London, Strand, London WC2R 2LS, United Kingdom

Koujin Takeda
Department of Computational Intelligence and Systems Science, Tokyo Institute of Technology, Yokohama 226-8502, Japan
and Department of Mathematics, King's College London, Strand, London WC2R 2LS, United Kingdom

(Received 13 March 2008; published 10 September 2008)

The spectral density of various ensembles of sparse symmetric random matrices is analyzed using the cavity method. We consider two cases: matrices whose associated graphs are locally treelike, and sparse covariance matrices. We derive a closed set of equations from which the density of eigenvalues can be efficiently calculated. Within this approach, the Wigner semicircle law for Gaussian matrices and the Marčenko-Pastur law for covariance matrices are recovered easily. Our results are compared with numerical diagonalization, showing excellent agreement.

DOI: 10.1103/PhysRevE.78.031116 PACS number(s): 46.65.+g, 89.20.−a, 89.75.Hc

I. INTRODUCTION

What started as an approximation to the complex Hamiltonian of heavy nuclei has become a very interesting area of research in its own right. Although the statistical properties of random matrices had been tackled before, it was that treatment by Wigner in nuclear physics during the 1950s which boosted the research into what is currently known as random matrix theory (RMT) [1]. The list of applications of this theory has been expanding ever since, ranging from physics to computer science and finance. Specifically, applications in physics include nuclear theory, quantum chaos, localization, theory of complex networks, and more (see, for instance, [2] for an extensive review).

From a theoretical and practical viewpoint, one of the central quantities of interest in RMT is the spectral density of an ensemble of random matrices. While some cases have been completely analyzed during the last decades, many others have not been fully explored. Consider, for instance, the ensemble of symmetric random matrices whose entries are independently and identically distributed Gaussian variables. Among many of its properties, it is well known that its spectral density is given by the Wigner semicircle law [1,3,4]. Another instance is the ensemble of covariance matrices, whose spectral density is given by the Marčenko-Pastur law [5]. And the list continues.

Interestingly, the change of introducing sparsity in such ensembles, i.e., many entries being zero, complicates the mathematical analysis enormously [6–10]. Lacking more powerful mathematical tools, one must rely on approximative schemes to the spectral density, e.g., the effective medium approximation (EMA), or the single defect approximation (SDA) [8–10].

In this work, we tackle the problem of evaluating the spectral density of sparse random matrices by using the cavity method [11,12]. As we will show, this approach may offer new theoretical and practical advantages: from a theoretical point of view, it offers an alternative, and we believe easier, method to (re)derive the spectral density; practically, the resulting cavity equations can be interpreted as a belief-propagation algorithm on single instances, which can be then easily implemented. The resulting spectral density is a clear improvement over those obtained by approximative schemes. A complementary study using the replica method and emphasizing ensemble aspects has been presented elsewhere [13].

This work is organized as follows. In Sec. II we first mention how the spectral density can be recast as a problem of interacting particles on a graph. The subsequent problem is then analyzed by the cavity method in two cases: locally treelike graphs and sparse covariance matrices. We derive cavity equations for large single instances and check that the dense limit gives the correct results. In Sec. III we use the cavity equations as an algorithm to calculate the spectral density and compare these results with numerical diagonalization. The last section is for conclusions.

II. CAVITY APPROACH TO THE SPECTRAL DENSITY

Consider an ensemble $\mathcal{M}$ of $N\times N$ symmetric matrices. If we denote by $\{\lambda_i^A\}_{i=1,\ldots,N}$ the set of eigenvalues of a given matrix $A\in\mathcal{M}$, its spectral density is defined as follows:

$$\varrho_A(\lambda)=\frac{1}{N}\sum_{i=1}^{N}\delta(\lambda-\lambda_i^A). \tag{1}$$

The spectral density of the ensemble, denoted as $\rho(\lambda)$, results from averaging $\varrho_A(\lambda)$ over $\mathcal{M}$. As was shown by Edwards and Jones [4], the density (1) can be rewritten as

$$\varrho_A(\lambda)=-\lim_{\epsilon\to 0^+}\frac{2}{\pi N}\mathrm{Im}\left(\frac{\partial}{\partial z}\ln\mathcal{Z}_A(z)\right)_{z=\lambda-i\epsilon}, \tag{2}$$

where

$$\mathcal{Z}_A(z)=\int\left(\prod_{i=1}^{N}\frac{dx_i}{\sqrt{2\pi}}\right)\exp\left(-\frac{1}{2}\sum_{i,j=1}^{N}x_i(zI-A)_{ij}x_j\right). \tag{3}$$

In writing the expression (3), we have been careless with the Gaussian integrals, so that as they stand they are not generally convergent; we simply follow the prescription as in

[14,15], and do not worry unnecessarily about imaginary factors, so that we can introduce a Gibbs-Boltzmann probability distribution of $\boldsymbol{x}$, viz.,

$$P_A(\boldsymbol{x}) = \frac{1}{\mathcal{Z}_A(z)} e^{-\mathcal{H}_A(\boldsymbol{x},z)} \tag{4}$$

with

$$\mathcal{H}_A(\boldsymbol{x},z) = \frac{1}{2} \sum_{(i,j)\in\mathcal{G}_A}^{N} x_i (zI - A)_{ij} x_j. \tag{5}$$

In this way, the spectral density $\varrho_A(\lambda)$ is recast into a statistical mechanics problem of N interacting particles $\boldsymbol{x} = (x_1, \ldots, x_N)$ on a graph $\mathcal{G}_A$ with effective Hamiltonian (5). By $\mathcal{G}_A$ we refer to a weighted graph with N nodes and edges for each interacting pair (i,j) with weight A_{ij}, when $A_{ij} \neq 0$. For later use, we introduce the following notation: the set of neighbors of a node i will be denoted as ∂i; for a given subset of nodes $\mathcal{B}$ we define $\boldsymbol{x}_{\mathcal{B}} = (x_{\ell_1}, \ldots, x_{\ell_{|\mathcal{B}|}})$ with $\ell_1, \ldots, \ell_{|\mathcal{B}|} \in \mathcal{B}$ and with $|\mathcal{B}|$ the number of nodes of $\mathcal{B}$; $k_i = |\partial i|$ denotes the number of neighbors of node i, while $c = (1/N)\Sigma_{i=1}^{N} k_i$ is the average connectivity. Note that within this approach Eq. (1) for the spectral density $\varrho_A(\lambda)$ can be rewritten as follows:

$$\varrho_A(\lambda) = \lim_{\epsilon \to 0^+} \frac{1}{\pi N} \sum_{i=1}^{N} \mathrm{Im}[\langle x_i^2 \rangle_z]_{z=\lambda - i\epsilon}, \tag{6}$$

where $\langle \cdots \rangle_z$ denotes the average over distribution (4).

In previous works [4,7–10], the averaged spectral density $\rho(\lambda)$ is dealt with by using the replica approach, or in [16,17] using supersymmetric methods. For general sparse matrices, it was shown in [7–10,16] that the analysis of the resulting equations from either the replica or the supersymmetric methods was a rather daunting task. To push the analysis further, the authors in [9,10] resorted to a series of approximative schemes, originally introduced in [8]. The simplest of such approximations, the EMA, assumes that all nodes are equivalent and play the same role [8–10]. This type of approximation works better the larger the average connectivity c of the graph. However, for low and moderate values of c it fails to provide an accurate description of the central part and the tails (see, for instance, [9]) and of the presence of weighted Dirac δ peaks in the spectral density [18,19]. Other approximations, like the SDA, also fail to give an accurate description of the spectrum.

To improve our understanding of spectral properties of sparse matrices, we tackle the problem from a different perspective. Instead of considering the averaged spectral density $\rho(\lambda)$, we note, as shown in Eq. (6), that to calculate $\varrho_A(\lambda)$ we simply need the local marginals $P_i(x_i)$ from the Gibbs-Boltzmann distribution $P_A(\boldsymbol{x})$. The cavity method offers a way to calculate them.[1] To illustrate this we consider two cases: the ensemble of symmetric locally treelike sparse matrices, and the ensemble of sparse covariance matrices.

[1]This approach was used in [23] within the context of Anderson localization.

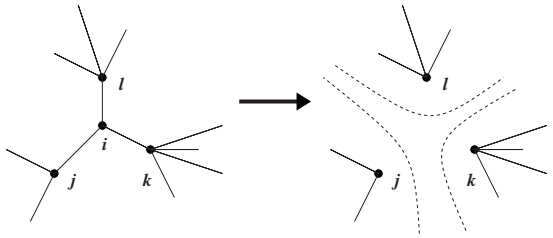

FIG. 1. Left: Part of a treelike graph $\mathcal{G}_A$ showing the neighborhood of node i. Right: Upon removal of node i, on the resulting cavity graph $\mathcal{G}_A^{(i)}$, the neighboring sites j, k, and l become uncorrelated.

A. Treelike symmetric matrices

Let us start by analyzing the spectral density of sparse graphs $\mathcal{G}_A$ which are treelike, like the one depicted in Fig. 1. By treelike, we mean that short loops are rare. Due to the treelike structure we note that, for each node i, the joint distribution of its neighborhood $P(\boldsymbol{x}_{\partial i})$ is correlated mainly through the node i. If, instead of the original graph $\mathcal{G}_A$, we consider a system where the node i is removed (see Fig. 1), on the resulting cavity graph $\mathcal{G}_A^{(i)}$ the joint distribution $P^{(i)}(\boldsymbol{x}_{\partial i})$ factorizes, i.e.,

$$P^{(i)}(\boldsymbol{x}_{\partial i}) = \prod_{\ell \in \partial i} P_\ell^{(i)}(x_\ell). \tag{7}$$

This factorization, which is exact on trees, is called the Bethe approximation. On the cavity graph, the set of cavity distributions $\{P_i^{(j)}(x_i)\}$ obeys simple recursive equations, viz.,

$$P_i^{(j)}(x_i) = \frac{e^{-z x_i^2/2}}{Z_i^{(j)}} \int d\boldsymbol{x}_{\partial i \setminus j} \exp\left(x_i \sum_{\ell \in \partial i \setminus j} A_{i\ell} x_\ell \right) \prod_{\ell \in \partial i \setminus j} P_\ell^{(i)}(x_\ell) \tag{8}$$

for all $i = 1, \ldots, N$ and for all $j \in \partial i$. Once the cavity distributions are known, the marginal distributions $P_i(x_i)$ of the original system $\mathcal{G}_A$ are given by

$$P_i(x_i) = \frac{e^{-z x_i^2/2}}{Z_i} \int d\boldsymbol{x}_{\partial i} \exp\left(x_i \sum_{\ell \in \partial i} A_{i\ell} x_\ell \right) \prod_{\ell \in \partial i} P_\ell^{(i)}(x_\ell) \tag{9}$$

for all $i = 1, \ldots, N$. While there is *in general* no *a priori* reason to expect cavity distributions to be simple, they are for the present system: the set (8) of equations is clearly self-consistently solved by Gaussian $P_i^{(j)}$'s. Hence, upon assuming the cavity distributions to be Gaussian, namely,

$$P_\ell^{(i)}(x) = \frac{1}{\sqrt{2\pi \Delta_\ell^{(i)}}} e^{-(1/2\Delta_\ell^{(i)}) x^2}, \tag{10}$$

the set of equations (8) is transformed into a set of equations for the cavity variances $\Delta_j^{(i)}(z)$, viz.,

$$\Delta_i^{(j)}(z) = \frac{1}{z - \Sigma_{\ell \in \partial i \setminus j} A_{i\ell}^2 \Delta_\ell^{(i)}(z)} \tag{11}$$

for all $i = 1, \ldots, N$ and for all $j \in \partial i$. Similarly, by Eq. (9) the marginals $P_i(x_i)$ are Gaussian with variance Δ_i related to the cavity variances by

$$\Delta_i(z) = \frac{1}{z - \Sigma_{\ell \in \partial i} A_{i\ell}^2 \Delta_\ell^{(i)}(z)}. \tag{12}$$

Equations (11) and (12) comprise the final result. For a given graph $\mathcal{G}_A$, one iterates the cavity Eq. (11) until convergence is reached. Once the cavity variances are known, the variances Δ_i are given by Eq. (12), from which the spectral density $\varrho_A(\lambda)$ is obtained by

$$\varrho_A(\lambda) = \lim_{\epsilon \to 0^+} \frac{1}{\pi N} \sum_{i=1}^{N} \mathrm{Im}[\Delta_i(z)]_{z=\lambda - i\epsilon}. \tag{13}$$

It is worth noting that equations equivalent to those in (11) can be derived by the method described in [20] and can be related to self-returning random walks [6,21].

Notice also that the set of cavity equations must be solved for complex $z=\lambda - i\epsilon$, so that the cavity variances are in general complex, and then the limit $\epsilon \to 0^+$ is performed. Instead, we perform this limit explicitly in the cavity equations. To do so, we separate these equations into their real and imaginary parts and then perform explicitly the limit $\epsilon \to 0^+$ by naively assuming that the imaginary part is nonvanishing in such a limit (see the discussion below). Denoting $(a_i^{(j)}, b_i^{(j)}) = [\mathrm{Re}(\Delta_i^{(j)}), \mathrm{Im}(\Delta_i^{(j)})]$, we obtain

$$a_i^{(j)} = \frac{\lambda - h_i^{(j)}(\boldsymbol{a})}{[\lambda - h_i^{(j)}(\boldsymbol{a})]^2 + [h_i^{(j)}(\boldsymbol{b})]^2}, \tag{14}$$

$$b_i^{(j)} = \frac{h_i^{(j)}(\boldsymbol{b})}{[\lambda - h_i^{(j)}(\boldsymbol{a})]^2 + [h_i^{(j)}(\boldsymbol{b})]^2}$$

with

$$h_i^{(j)}(\boldsymbol{v}) = \sum_{\ell \in \partial i \setminus j} A_{i\ell}^2 v_\ell^{(i)}. \tag{15}$$

Our results are exact, as long as the average connectivity c of the graphs considered remains finite in the limit $N \to \infty$.

Large-c limit: The Wigner semicircle law

To assess our approach, note that from the set of equations (11) and (12) we can easily recover the Wigner semicircle law in the large-c limit. By this limit we understand that $k_i \to c$ and $c \to \infty$, and assume that the graph is already "infinitely" large.[2] To perform this large-c limit, we take the entries of the matrix A to be $A_{ij} = J_{ij}/\sqrt{c}$, with J_{ij} $(=J_{ji})$ a Gaussian variable with zero mean and variance J^2. From Eqs. (11) and (12), we note that, for large c, we have that $\Delta_i^{(j)}(z) = \Delta_i(z) + O(c^{-1})$.[3] Upon defining

[2]Alternatively, one could naively take $c \to N$ and then $N \to \infty$. In the complete, or fully connected, graph $(c=N)$ the cavity equations are still valid, but the reason for the decorrelation is statistical rather than topological.

[3]This is the usual derivation of Thouless-Anderson-Palmer (TAP) equations from the cavity equations. In this case the difference between cavity fields and effective fields does not produce an Onsager reaction term.

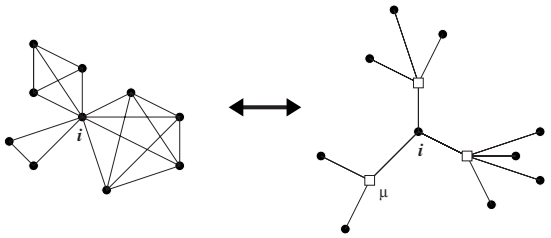

FIG. 2. Left: Graph $\mathcal{G}_A$ for covariance matrices. Right: Bipartite graph $\mathcal{G}_{\boldsymbol{\xi}}$ for the matrix $\boldsymbol{\xi}$. For sake of clarity, self-interactions in the graph $\mathcal{G}_A$ are not drawn.

$$\Delta = \lim_{c \to \infty} \frac{1}{c} \sum_{\ell \in \partial i} \Delta_\ell, \tag{16}$$

we obtain that

$$\lim_{c \to \infty} \sum_{\ell \in \partial i} A_{i\ell}^2 \Delta_\ell^{(i)} = \lim_{c \to \infty} \frac{1}{c} \sum_{\ell \in \partial i} J_{i\ell}^2 \Delta_\ell^{(i)} = J^2 \Delta. \tag{17}$$

Thus, in the large-c limit, Eq. (12) yields

$$\Delta = \frac{1}{z - J^2 \Delta}, \tag{18}$$

which gives the well-known Wigner semicircle law [3]

$$\rho(\lambda) = \frac{1}{2\pi J^2} \sqrt{4J^2 - \lambda^2}. \tag{19}$$

B. Covariance matrices

Let us consider now matrices A of the type

$$A_{ij} = \frac{1}{d} \sum_{\mu=1}^{P} \xi_{i\mu} \xi_{j\mu}, \tag{20}$$

where $\boldsymbol{\xi}$ is an $N \times P$ matrix with entries $\xi_{i\mu}$. To this matrix we can associate a bipartite graph $\mathcal{G}_\xi$ with $N+P$ nodes, divided into two sets indexed by $i=1,\ldots,N$ and $\mu=1,\ldots,P$ (see Fig. 2). A pair of nodes (i,μ) is connected if $\xi_{i\mu} \neq 0$. We refer to these nodes as $\boldsymbol{x}$ nodes and $\boldsymbol{m}$ nodes, respectively. We will consider the bipartite graph $\mathcal{G}_{\boldsymbol{\xi}}$ to be treelike, i.e., many of the entries $\xi_{i\mu}$ are zero. We also introduce $d = (1/P)\Sigma_{\mu=1}^{P} k_\mu$ with $k_\mu = |\partial\mu|$, i.e., the average connectivity of the $\boldsymbol{m}$ nodes. Clearly, $c = \alpha d$ with $\alpha = P/N$. In this case it is more convenient to apply the cavity method on the bipartite graph $\mathcal{G}_{\boldsymbol{\xi}}$. To do so we write the effective Hamiltonian (5) as follows:

$$\mathcal{H}_A(\boldsymbol{x}, z) = \frac{1}{2} z \sum_{i=1}^{N} x_i^2 - \frac{1}{2} \sum_{\mu=1}^{P} m_\mu^2(\boldsymbol{x}_{\partial\mu}), \tag{21}$$

where we have defined the overlaps

$$m_\mu(\boldsymbol{x}_{\partial\mu}) = \frac{1}{\sqrt{d}} \sum_{i \in \partial\mu} \xi_{i\mu} x_i. \tag{22}$$

Note that, due to our choice for $\boldsymbol{\xi}$ and the relation (20) between the matrices A and $\boldsymbol{\xi}$, the corresponding graph $\mathcal{G}_A$ (see Fig. 2) is locally cliquelike with self-interactions.

We work our cavity equations in the bipartite graph $\mathcal{G}_{\boldsymbol{\xi}}$. Here, the variables $\boldsymbol{x}$ are on the $\boldsymbol{x}$ nodes while the variables $\boldsymbol{m}=(m_1,\ldots,m_p)$ are on the $\boldsymbol{m}$ nodes. Since we have two types of nodes, we apply the cavity method twice: around $\boldsymbol{x}$ nodes and around $\boldsymbol{m}$ nodes. We define $Q_\nu^{(i)}(m_\nu)$ as the cavity distribution of m_ν in the absence of a node i, and $P_i^{(\mu)}(x_i)$ is the cavity distribution of x_i in the absence of node μ. We find the following set of equations for these cavity distributions:

$$P_i^{(\mu)}(x_i)=\frac{e^{-zx_i^2/2}}{Z_i^{(\mu)}}\int d\boldsymbol{m}_{\partial i\backslash\mu}\exp\left[\frac{1}{2}\sum_{\nu\in\partial i\backslash\mu}\left(m_\nu+\frac{1}{\sqrt{d}}\xi_{i\nu}x_i\right)^2\right]\times\prod_{\nu\in\partial i\backslash\mu}Q_\nu^{(i)}(m_\nu) \tag{23}$$

for all $i=1,\ldots,N$ and $\mu\in\partial i$. Also,

$$Q_\nu^{(i)}(m_\nu)=\frac{1}{Z_\nu^{(i)}}\int d\boldsymbol{x}_{\partial\nu\backslash i}\delta\left(m_\nu-\frac{1}{\sqrt{d}}\sum_{\ell\in\partial\nu\backslash i}\xi_{\ell\nu}x_\ell\right)\times\prod_{\ell\in\partial\nu\backslash i}P_\ell^{(\nu)}(x_\ell) \tag{24}$$

for all $\nu=1,\ldots,P$ and $i\in\partial\nu$. Obviously, for the marginal distributions $P_i(x_i)$ we obtain

$$P_i(x_i)=\frac{e^{-zx_i^2/2}}{Z_i}\int d\boldsymbol{m}_{\partial i}\exp\left[\frac{1}{2}\sum_{\nu\in\partial i}\left(m_\nu+\frac{1}{\sqrt{d}}\xi_{i\nu}x_i\right)^2\right]\times\prod_{\nu\in\partial i}Q_\nu^{(i)}(m_\nu) \tag{25}$$

for all $i=1,\ldots,N$. As before, we see from the set of equations (23) and (24) that the Gaussian measure is a fixed point. Thus, by taking $P_i^{(\mu)}(x_i)$ and $Q_\mu^{(i)}(m_\mu)$ to be Gaussian distributions with zero mean and variances $\Delta_i^{(\mu)}$ and $\Gamma_\mu^{(i)}$, respectively, we obtain the following set of equations for the cavity variances

$$\Delta_i^{(\mu)}(z)=\frac{1}{z-\frac{1}{d}\Sigma_{\nu\in\partial i\backslash\mu}\xi_{i\nu}^2\frac{1}{1-\Gamma_\nu^{(i)}(z)}},$$

$$\Gamma_\nu^{(i)}(z)=\frac{1}{d}\sum_{\ell\in\partial\nu\backslash i}\xi_{\ell\nu}^2\Delta_\ell^{(\nu)}(z). \tag{26}$$

Similarly, if we denote with Δ_i the variance of the marginal $P_i(x_i)$ on the original graph $\mathcal{G}_{\boldsymbol{\xi}}$, we obtain

$$\Delta_i(z)=\frac{1}{z-\frac{1}{d}\Sigma_{\nu\in\partial i}\xi_{i\nu}^2\frac{1}{1-\Gamma_\nu^{(i)}(z)}}. \tag{27}$$

Large-c limit: The Marčenko-Pastur law

For the sake of simplicity we take the nonzero entries of the matrix $\boldsymbol{\xi}$ to have values ±1, so that $\xi_{i\mu}^2=1$ in Eqs. (26) and (27). Let us consider the spectral density in the large-c limit of the bipartite graph $\mathcal{G}_{\boldsymbol{\xi}}$. By this limit we mean $k_\mu\to d$, $k_i\to c$, and $d,c\to\infty$ while α remains finite. As before, the difference between cavity variances and variances is $O(c^{-1})$. If we define

$$\Delta=\lim_{d\to\infty}\frac{1}{d}\sum_{\ell\in\partial\nu}\Delta_\ell=\lim_{d\to\infty}\frac{1}{d}\sum_{\ell=1}^{d}\Delta_\ell \tag{28}$$

from Eq. (27) we obtain

$$\Delta=\frac{1}{z-\alpha\frac{1}{1-\Delta}}. \tag{29}$$

Upon solving this equation for $\mathrm{Im}(\Delta)$ we obtain the Marčenko-Pastur law [5] of dense covariance matrices,

$$\rho(\lambda)=\frac{1}{2\pi\lambda}\sqrt{-\lambda^2+2\lambda(\alpha+1)+(\alpha-1)^2}+C_0(1-\alpha)\delta(\lambda), \tag{30}$$

with $C_0=1$ for $\alpha\leqslant1$ and $C_0=0$ for $\alpha>1$. A slightly different expression is found by Nakanishi and Takayama [22], where the difference comes from not considering the diagonal terms. This could also be implemented fairly straightforwardly to obtain the spectral density as in [22].

III. NUMERICAL RESULTS AND COMPARISON

For general sparse matrices, we solve the cavity equations numerically and compare the results with exact numerical diagonalization. We consider again the two cases of locally treelike and sparse covariance matrices.

A. Treelike symmetric matrices

To test our cavity equations, we choose Poissonian graphs $\mathcal{G}_A$ where each entry A_{ij} of the $N\times N$ matrix A is drawn independently from

$$P(A_{ij})=\frac{c}{N}\pi(A_{ij})+\left(1-\frac{c}{N}\right)\delta(A_{ij}) \tag{31}$$

with c the average connectivity, and $\pi(x)$ is the distribution of nonzero edge weights. For the distribution of weights we study two cases: the bimodal distribution, i.e.,

$$\pi(A_{ij})=\frac{1}{2}\delta(A_{ij}-1)+\frac{1}{2}\delta(A_{ij}+1), \tag{32}$$

and the Gaussian distribution with zero mean and variance $1/c$.

For the purpose of fairly comparing later with exact numerical diagonalization, we have analyzed the cavity equations for rather small matrices. However, we have checked that the convergence of these equations is generally fairly fast and we are able to evaluate the spectral density of very large matrices in reasonable time. In both the bimodal and the Gaussian cases, we generated matrices with $N=1000$. For each matrix we run our cavity equations (11) until convergence is reached and then obtain the spectral density from Eqs. (12). The result is averaged over 1000 samples. For such sizes we have also calculated the spectral density by exact numerical diagonalization and averaged over 1000 samples.

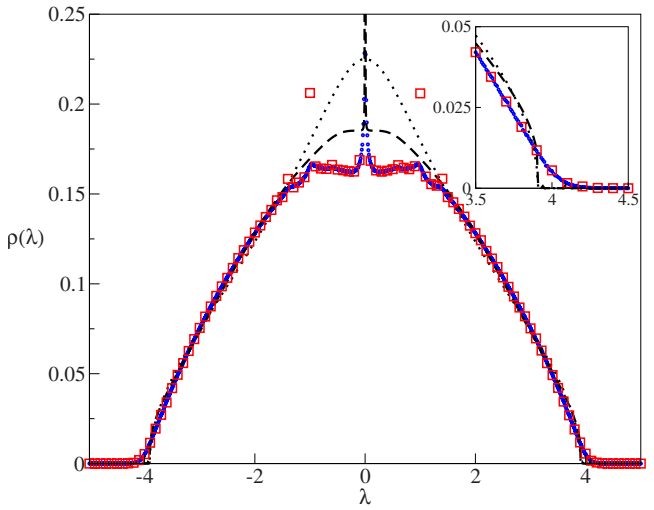

FIG. 3. (Color online) Spectral density of Poissonian graphs with bimodal edge weights and average connectivity $c=3$. Red square markers are the results of numerical diagonalization with $N=1000$, averaged over 1000 samples. Blue circles are the results of the cavity approach with $N=1000$, averaged over 1000 samples. The dashed line corresponds to the SDA and the dotted line is the EMA. The inset shows the tail of the spectral density.

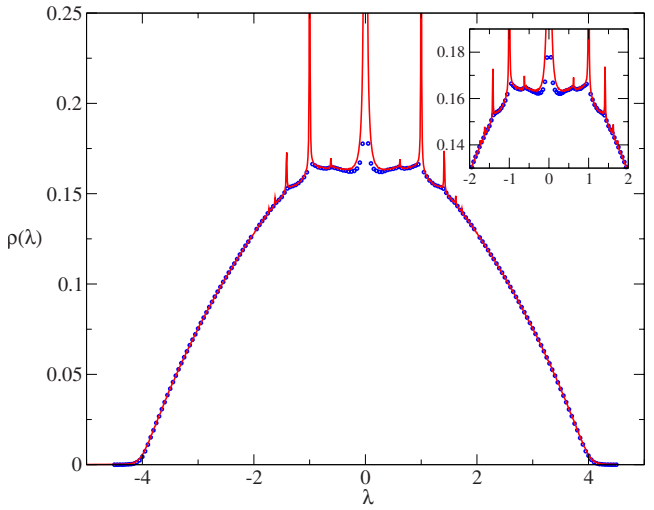

FIG. 4. (Color online) Comparison of cavity equations for $\epsilon=0$ (blue circles) and 0.005 (continuous red line), for Poissonian graphs with bimodal edge weights and average connectivity $c=3$ ($N=1000$ and average over 1000 samples). The inset shows the Dirac δ structure in the central region.

The numerical results from the cavity approach and exact numerical diagonalization for the bimodal case are plotted in Fig. 3 for average connectivity $c=3$. We have also compared our results with the spectral density obtained by the EMA and SDA (see [6,8,9] for details about the approximations). As we can see, our results are a clear improvement over the EMA and SDA results, as they are in excellent agreement with numerical diagonalization. Even the tail of the spectrum, usually not obtained with these approximations, (see inset of Fig. 3), is well reproduced by our approach.

It is well known that the spectrum of these types of ensembles contains a dense collection of Dirac δ peaks [18,19], which are not fully captured by the previous approximations. Without a prior analysis, one wonders how the cavity equations can be used to obtain such contributions. A practical way out is to reconsider the limit $\epsilon \to 0$, by leaving a small value of ϵ in the cavity equations, which implies approximating Dirac δ's by Lorentzian peaks. In Fig. 4 we have rerun the set of equations (11) and (12) with a small value of ϵ. The Dirac δ contributions, whose exact positions within the spectral density are discussed in [18], are now clearly visible. A more detailed study on this issue within the context of localization can be found in [13].

In Fig. 5 we plot the results of both numerical diagonalization and the cavity method when $\pi(x)$ is a Gaussian distribution with zero mean and variance $1/c$. Once again, our results are in excellent agreement with the numerical simulations.

B. Covariance matrices

We have also analyzed numerically in the case of sparse covariance matrices. Here the entries $\xi_{i\mu}$ of the $N \times P$ matrix $\boldsymbol{\xi}$ are drawn according to the distribution

$$P(\xi_{i\mu}) = \frac{d}{N}\pi(\xi_{i\mu}) + \left(1 - \frac{d}{N}\right)\delta(\xi_{i\mu}), \tag{33}$$

where $\pi(\xi_{i\mu})$ is a bimodal distribution,

$$\pi(\xi_{i\mu}) = \frac{1}{2}\delta(\xi_{i\mu} + 1) + \frac{1}{2}\delta(\xi_{i\mu} - 1). \tag{34}$$

In Fig. 6, we compare the results of direct diagonalization, the cavity method, and the symmetric effective medium approximation (SEMA), introduced in [10]; here we make the same choice of parameters. The inset figure shows details of

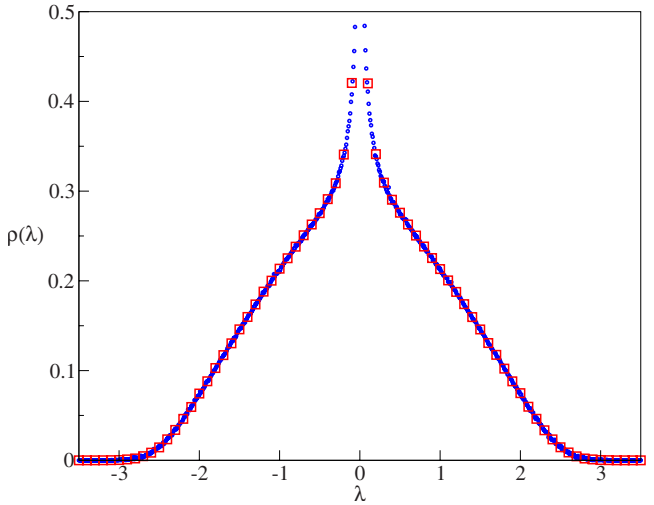

FIG. 5. (Color online) Spectral density of Poissonian graphs with Gaussian edge weights and average connectivity $c=4$. Red square markers are for the results of numerical diagonalization with $N=1000$, averaged over 1000 samples. Blue circles are results of the cavity approach with $N=1000$ and average over 1000 samples.

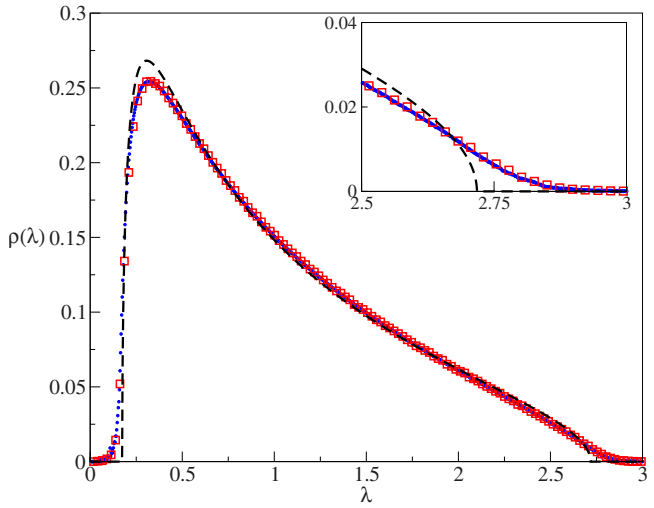

FIG. 6. (Color online) Spectral density of covariance matrices with $N=4000$, $d=12$, $\alpha=0.3$. Average over 1000 samples. Red square markers are for the results of numerical diagonalization. Blue circles are results of the cavity approach. The dashed line corresponds to the SEMA.

the tail region of the plot, where the difference between the SEMA and the other results can be clearly seen.

IV. CONCLUSIONS

In this work, we have reexamined the spectral density of ensembles of sparse random symmetric matrices. By following Edwards and Jones [4], we have mapped the problem into an interacting system of particles on a sparse graph, which was then analyzed by the cavity approach. Within this framework, we have derived cavity equations on single instances and used them to calculate the spectral densities of sparse symmetric matrices. Our results are in good agreement with numerical diagonalization and are a clear improvement to previous works based on approximative schemes. We have also shown that, to account for the Dirac δ contribution to the spectrum, one may approximate Dirac δ peaks by Lorentzians, by leaving a small value for ϵ [13].

It is well known that cavity and replica methods are equivalent (see, for instance, [12] for diluted spin glasses), so one may wonder in which aspects our work differs from the ones presented in [7–10]. Generally, for interacting diluted systems with continuous dynamical variables, one expects an infinite number of cavity fields to parametrize the cavity distributions. The authors in [7–10] decided to tackle such a daunting task by resorting to approximations. In this work, we simply realize that, for the problem at hand, the cavity distributions are Gaussian, so that the problem can be solved exactly by self-consitently determining the variances of these distributions.

In future studies we expect to extend the method presented here to the analysis of more general aspects of random matrices.

ACKNOWLEDGMENTS

K.T. acknowledges hospitality from the Disordered Systems Group, at the department of Mathematics, King's College London. He was supported by a Grand-in-Aid from MEXT/JSPS, Japan (No. 18079006) and the Program for Promoting Internationalization of University Education, MEXT, Japan (Support for Learning Overseas Advanced Practices in Research). The authors thank M. Mézard and Y. Kabashima for discussions and G. Parisi for discussions and for pointing out earlier work on the subject. I.P.C. also thanks A. C. C. Coolen for his work during the initial stages of this Guzai project.

[1] M. L. Mehta, *Random Matrices* (Academic, New York, 1991).
[2] T. Guhr, A. Müller-Groeling, and H. A. Weidenmüller, Phys. Rep. **299**, 190 (1998).
[3] E. P. Wigner, Ann. Math. **67**, 325 (1958).
[4] S. F. Edwards and R. C. Jones, J. Phys. A **9**, 1595 (1976).
[5] V. A. Marčenko and L. A. Pastur, Math. USSR. Sb. **1**, 457 (1967).
[6] S. N. Dorogovtsev, A. V. Goltsev, J. F. F. Mendes, and A. N. Samukhin, Phys. Rev. E **68**, 046109 (2003).
[7] G. J. Rodgers and A. J. Bray, Phys. Rev. B **37**, 3557 (1988).
[8] G. Biroli and R. Monasson, J. Phys. A **32**, L255 (1999).
[9] G. Semerjian and L. F. Cugliandolo, J. Phys. A **35**, 4837 (2002).
[10] T. Nagao and T. Tanaka, J. Phys. A **40**, 4973 (2007).
[11] M. Mezard, G. Parisi, and M. Virasoro, *Spin Glass Theory and Beyond*, World Scientific Lecture Notes in Physics Vol. 9 (World Scientific, Singapore, 1987).
[12] M. Mezard and G. Parisi, Eur. Phys. J. B **20**, 217 (2001).
[13] R. Kühn, J. Phys. A **41**, 295002 (2008).
[14] G. P. M. Mezard and A. Zee, Nucl. Phys. B **559**, 689 (1999).
[15] G. Parisi, in *Applications of Random Matrices in Physics*, NATO Science Series II: Mathematics, Physics, and Chemistry, edited by E. Brezin, V. Kazakov, D. Serban, P. Wiegmann, and A. Zabrodin (Springer, Berlin, 2006), p. 219.
[16] Y. V. Fyodorov and A. D. Mirlin, J. Phys. A **24**, 2219 (1991).
[17] G. J. Rodgers and C. D. Dominicis, J. Phys. A **23**, 1567 (1990).
[18] O. Golinelli, e-print arXiv:cond-mat/0301437.
[19] M. Bauer and O. Golinelli, J. Stat. Phys. **103**, 301 (2001).
[20] R. Abou-Chacra, D. J. Thouless, and P. W. Anderson, J. Phys. C **6**, 1734 (1973).
[21] D. M. Malioutov, J. K. Johnson, and A. S. Willsky, J. Mach. Learn. Res. **7**, 2031 (2006).
[22] K. Nakanishi and H. Takayama, J. Phys. A **30**, 8085 (1997).
[23] S. Ciliberti, T. S. Grigera, V. Martin-Mayor, G. Parisi, and P. Verrocchio (unpublished).